DNS of square-cylinder flow using hybrid wavelet-collocation/volume-penalization method

G. De Stefano and O.V. Vasilyev

1 Introduction

The direct numerical simulation (DNS) of unsteady flow past a square-cylinder has a very high computational cost, even at moderately low Reynolds-numbers (Re), where the transition to a complex 3D wake occurs. In fact, the cylinder wake is unstable to two main spanwise disturbances that are referred to as "Mode A" and "Mode B" in the literature, similarly to what happens for circular cylinders. For the long-wavelength Mode A, the critical Re has been observed to be around 160, while the short-wavelength Mode B has been found to become unstable for Re $\approx$ 190. The spanwise wavelengths of the above two modes are about 5.2 and 1.2 times the side length of the cross section, respectively [1].

In order to numerically predict the essential features of the transitional shedding flow past the cylinder, the extent of the computational domain in the homogeneous spanwise direction, where periodic boundary conditions are applied, must be sufficiently high to capture the evolution of the 3D disturbances. Furthermore, the numerical grid must be properly refined close to the body surface, to resolve the boundary layer, as well as in the wake region. The degrees of freedom of the solution and, thus, the associated computational cost can be drastically reduced by using adaptive numerical methods, where the spatially non-uniform grid is not prescribed *a-priori* but dynamically adapted following the flow evolution.

In this study, the mesh adaptation is based on the wavelet decomposition of the velocity field, by automatically refining the grid where high gradients in the solution exist. The wavelet-based eddy-capturing approach [2] is extended to non-homogeneous bluff-body flow, where the presence of the obstacle is mimicked by using the Brinkman volume-penalization method [3].

Giuliano De Stefano
DIII, Seconda Università di Napoli, I 81031, Italy, e-mail: giudeste@unina.it

Oleg V. Vasilyev
DME, University of Colorado, CO 80309, USA, e-mail: oleg.vasilyev@colorado.edu

2 Hybrid method

The volume-penalization approach results in slightly modifying the governing equations with the addition of an appropriate forcing term, without altering the underlying numerical grid. Instead of solving the incompressible Navier-Stokes equations in the fluid domain $\Omega_{\rm f}$, with the associated no-slip BC on the body surface $\partial\Omega_{\rm s}$, the following (dimensionless) governing equations for the penalized velocity field $\tilde{u}_i$ are solved in the entire domain $\Omega = \Omega_{\rm f} \bigcup \Omega_{\rm s}$:

$$\frac{\partial \tilde{u}_i}{\partial x_i} = 0\,, \tag{1}$$

$$\frac{\partial \tilde{u}_i}{\partial t} + (\tilde{u}_j + U_j)\frac{\partial \tilde{u}_i}{\partial x_j} = -\frac{\partial \tilde{p}}{\partial x_i} + \frac{1}{\mathrm{Re}}\frac{\partial^2 \tilde{u}_i}{\partial x_j \partial x_j} - \frac{\chi_{\rm s}}{\eta}(\tilde{u}_i + U_i)\,. \tag{2}$$

The imposed uniform velocity field U_j corresponds to the given freestream velocity. The additional term at the RHS of the penalized momentum equation (2) mimics the presence of a porous obstacle, where $\chi_{\rm s}$ stands for the mask function associated with the obstacle domain $\Omega_{\rm s}$.

The positive constant η, which has the dimension of time and reflects the fictitious porousness of the obstacle, stands for the key-parameter in the volume-penalization approach. For vanishing η, the solution $\tilde{u}_i$ of the penalized equations (1) and (2) converges to the solution of the original equations with the global penalization error scaling as $\eta^{1/2}$ in $\Omega_{\rm f}$. Therefore, the no-slip BC can be enforced to any desired accuracy by appropriately reducing the penalization parameter. In addition, the Brinkman approach is particularly advantageous because the aerodynamic force acting on the obstacle can be simply evaluated as

$$F_i(t) = \frac{1}{\eta}\int_{\Omega_s} (\tilde{u}_i + U_i) d\mathbf{x}\,, \tag{3}$$

i.e., by integrating the total velocity field over the volume occupied by the obstacle.

Generally, the continuity (1) and penalized Navier-Stokes (2) equations could be solved with any numerical technique. In this work, the efficient combination of the volume-penalization approach with the adaptive wavelet-collocation (AWC) solver is used [4]. The governing equations are evaluated at collocation points, which leads to a set of nonlinear ODEs for the collocated velocity unknowns. The method allows the numerical grid to be dynamically adapted in time, following the evolution of the dominant flow structures, which are unambiguously identified and tracked during the simulation. Namely, the mesh adaptation is obtained through the use of nested wavelet grids, owing to the one-to-one correspondence between wavelets and grid points. The method is particularly effective in the simulation of shedding flow past bluff bodies, where the wavelet-based adaptation allows the grid to be continuously modified in time in order to follow the space-time evolution of the wake.

Formally, the perturbation velocity field, $\tilde{u}_i(\mathbf{x})$, is decomposed in terms of wavelet basis functions and approximated by retaining only significant wavelets:

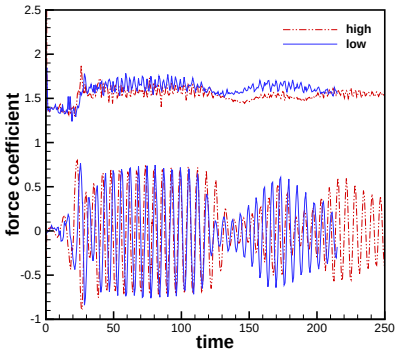

Fig. 1 Time-history of the drag (top) and lift (down) coefficient for two different wavelet thresholding levels that are $\varepsilon = 0.01$ (lower) and 0.005 (higher accuracy).

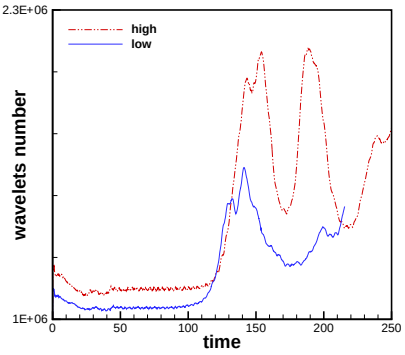

Fig. 2 Time-history of the number of retained wavelets for two different wavelet thresholding levels that are $\varepsilon = 0.01$ (lower) and 0.005 (higher accuracy).

$$\tilde{u}_i(\mathbf{x}) \cong \sum_{\mathbf{l}\in\mathscr{L}^0} c_{\mathbf{l}}^0 \phi_{\mathbf{l}}^0(\mathbf{x}) + \sum_{j=0}^{+\infty} \sum_{\mu=1}^{2^n-1} \sum_{\substack{\mathbf{k}\in\mathscr{K}^{\mu,j} \\ |d_{\mathbf{k}}^{\mu,j}|>\varepsilon|u_i|}} d_{\mathbf{k}}^{\mu,j} \psi_{\mathbf{k}}^{\mu,j}(\mathbf{x}). \tag{4}$$

Each level of resolution j consists of wavelets belonging to the same family, having the same scale but located at different grid positions. Collocation points are in fact omitted from the computational grid if the associated wavelets are omitted from representation (4), which occurs when the corresponding coefficients are below the given thresholding level. In a practical calculation, the level of resolution is bounded so that $j \leq j_{\max}$, where the choice of the maximum resolution, which corresponds to the finest allowable wavelet grid, is dictated by the physically required spatial resolution as well as the acceptable computational cost. Depending on the choice of the parameter ε, only a small fraction of the available wavelets is used in representing the velocity field $\tilde{u}_i$, which results in the characteristic compression property of the wavelet-based methods [5]. The thresholding level ε determines the relative energy level of the eddies that are resolved and, consequently, controls the importance of the residual field associated with the discarded wavelets. A very low but non-zero value for this parameter can be prescribed so that the effect of unresolved motions can be completely ignored and the wavelet-based DNS solution of the penalized equations (2) is carried out, like it happens for the present study.

When combining the AWC method with the volume-penalization technique, the presence of the cylinder is automatically taken into account by adapting the computational mesh on the penalized velocity field and, possibly, the mask function.

3 Square-cylinder flow

The hybrid method presented above is applied to the simulation of vortex shedding behind a stationary right prism with square cross-section, immersed in a uniform fluid stream. The flow around the cylinder is described in a Cartesian coordinate system (x,y,z), where the first axis corresponds to the inlet flow direction and the third one coincides with the spanwise direction. The computational domain is chosen to be $\Omega = [-6,18]\times[-9,9]\times[-3,3]$, while the domain occupied by the cylinder is $\Omega_{\rm s} = [-0.5,0.5]\times[-0.5,0.5]\times[-3,3]$, the side length of the square-section being assumed as reference length. Zero-velocity conditions are imposed at the inflow boundary ($x=-6$), while convective conditions are prescribed at the outflow boundary ($x=18$). Free-slip conditions are imposed at the lateral boundaries ($y=\pm 9$), i.e. $\partial\tilde{u}_1/\partial y = \tilde{u}_2 = \partial\tilde{u}_3/\partial y = 0$, and periodicity is assumed in the homogeneous spanwise direction ($z=\pm 3$).

The DNS of square-cylinder transitional flow at Re=200 is obtained starting from zero perturbation velocity. The incoming flow is undisturbed and the transition is naturally promoted by the numerical truncation errors. The penalization parameter is set to $\eta = 0.001$, while two different thresholding levels, namely, $\varepsilon = 0.005$ and $\varepsilon = 0.01$, and seven levels of resolution ($1 \le j \le 7$) are used for the AWC solver. Here, differently from similar studies, the non-uniform mesh spacing is not prescribed *a-priori*, but dynamically determined according to the flow evolution. In particular, close to the body surface, the local resolution is dictated by the high gradients of the mask function $\chi_{\rm s}$ and, thus, the finest wavelet collocation grid is used. Due to the moderately low Re, the prescribed maximum resolution is adequate to resolve the kinematic boundary layer inside the fluid region.

After a transient period, during which the wake develops from initial free-stream conditions, the aerodynamic forces exhibit the classical oscillatory behavior of bluff-body flows, as illustrated in Fig. 1, where the time histories of the spanwise-averaged drag and lift coefficient are reported. In the higher accuracy case, the time-averaged drag-coefficient is $\overline{C}_D = 1.54$ and the associated RMS value is $C'_D = 0.027$ while, for the lift-coefficient, it holds $|\overline{C}_L| = 5.3\times 10^{-3}$ and $C'_L = 0.31$. The fundamental frequency of vortex shedding corresponds to the Strouhal-number ${\rm St} = f_0 L/U = 0.15$. The present global results are in good agreement with solutions provided by different non-adaptive DNS solutions, e.g. [1], as well as experimental findings, e.g. [6].

The flow dynamics is governed by the vortical structures that are shed from the cylinder and convected downstream, while secondary vortices are generated in the near wake. During a high-force phase, like for instance at $t \cong 175$, the wake is characterized by the presence of large spanwise vortices. Eventually, these structures are destroyed and, during a low-force phase, like for instance at $t \cong 190$, the wake shows a complex 3D shape due to symmetric two-sided dislocation. It appears that the time history of the retained wavelets number reflects the oscillations of the wake-induced forces, as demonstrated in Fig. 2.

In order to present a clear 3D view of the cylinder wake, the main vortical structures can be identified according to the *Q-criterion*, which simply defines a vortex

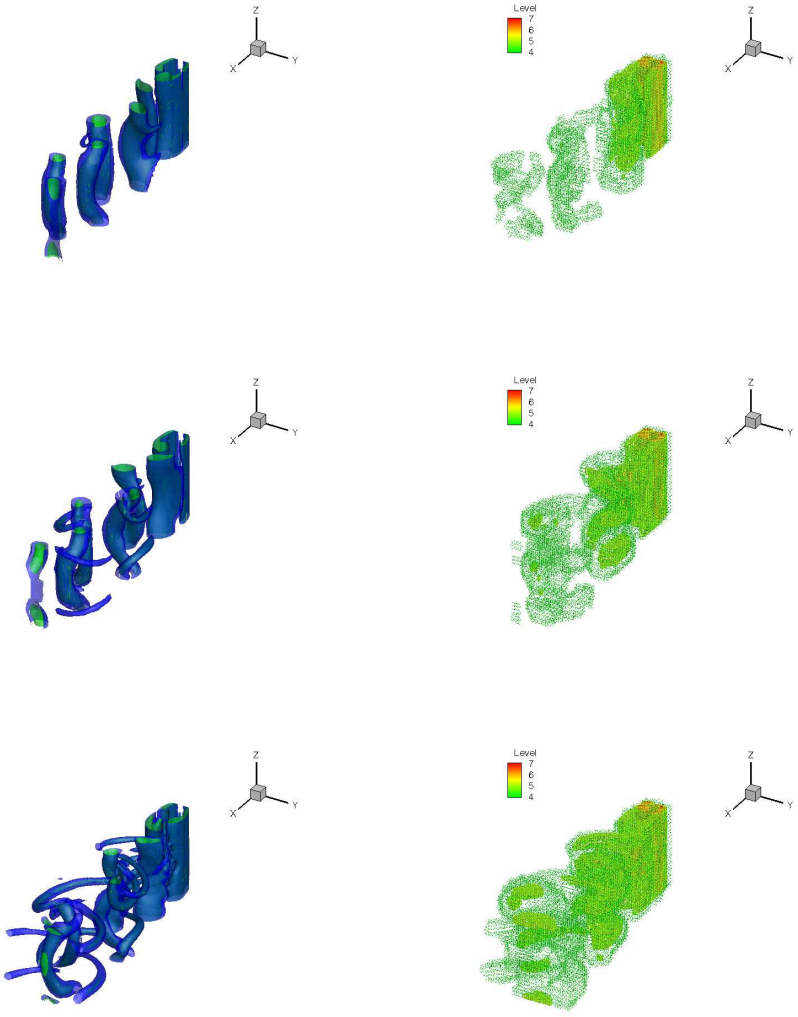

Fig. 3 Main vortical structures identified by the iso-surfaces of $Q = 0.1$ (blue) and 0.3 (green), on the left, and scatter plot of the wavelet collocation points at higher levels of resolution ($4 \leq j \leq 7$), on the right. Close-up view in the domain: $-2 < x < 17$, $-3 < y < 3$, $-3 < z < 3$, at three different time instants.

as a connected region with a positive second invariant of the velocity-gradient tensor, e.g. [7]. The evolution of the wake is visualized on Fig. 3, by reporting three different pictures at three different time instants. The iso-surfaces of $Q = 0.1$ and 0.3 are drawn (on the left of the figure) along with the scatter plot (on the right)

of the collocation points associated to the retained wavelets. Since all the wavelets belonging to the coarser levels of resolution with $j \leq 3$ are actually kept throughout the computational domain, for the sake of clarity, the scatter plot, which is colored by the variable grid level, is reported only for $4 \leq j \leq 7$.

In fact, the number and the spatial distribution of the retained wavelet collocation points follow the evolution of the wake. During a period of high force, the rather simple wake can be simulated by using a relatively low number of wavelets. On the contrary, during a period of low force, which corresponds to a very complex shape of the wake, much more grid-points are included in the computation as the wavelet collocation grid is automatically refined where smaller vortical structures are created.

4 Concluding remarks

The application of the hybrid volume-penalization/wavelet-collocation method to the simulation of unsteady 3D incompressible square-cylinder transitional flow is presented. The method allows the adaptive DNS to be performed with a reasonable computational cost, while directly controlling the errors in the numerical approximation. Due to its flexibility and efficiency, the proposed combined method appears very promising for the simulation of more challenging flows. For instance, higher Re and/or more complex geometry bluff body flows could be considered, where the adaptive wavelet-based method are expected to become even more efficient.

Acknowledgements The support by the US NSF under grant No. CBET-1236505 is gratefully acknowledged. Authors are also thankful for the computing time on the Janus supercomputer, which is a joint effort of the University of Colorado and the National Center for Atmospheric Research.

References

1. Robichaux, J., Balachandar, S., Vanka, S.P.: Three-dimensional Floquet instability of the wake of square cylinder. Phys. Fluids **11**, 560–578 (1999)
2. De Stefano, G., Vasilyev, O. V.: A fully adaptive wavelet-based approach to homogeneous turbulence simulation. J. Fluid Mech. **695**, 149–172 (2012)
3. Angot, P., Bruneau, C.-H., Fabrie, P.: A penalization method to take into account obstacles in viscous flows. Numer. Mat. **81**, 497–520 (1999)
4. Kevlahan, N. K.-R., Vasilyev, O. V.: An adaptive wavelet collocation method for fluid-structure interaction at high Reynolds numbers. SIAM J. Sc. Comp. **26**, 1894–1915 (2005)
5. Schneider, K., Vasilyev, O. V.: Wavelet methods in computational fluid dynamics. Ann. Rev. Fluid Mech. **42**, 473–503 (2010)
6. Okajima, A.: Strouhal numbers of rectangular cylinders. J. Fluid Mech. **123**, 379–398 (1982)
7. De Stefano, G., Denaro, F. M., Riccardi, G.: High order filtering for control volume flow simulations. Int. J. Num. Meth. Fluids **37**, 797–835 (2001)